The axial methionine ligand may control the redox reorganizations in the active site of blue copper proteins

Koji Ando[a)]
Department of Chemistry, Graduate School of Science, Kyoto University, Sakyo-ku, Kyoto 606-8502, Japan

(Received 22 June 2010; accepted 10 September 2010; published online 2 November 2010)

Structural and energetic reorganizations in redox reaction of type 1 copper proteins are studied by density functional and *ab initio* molecular orbital calculations. Model complexes of the active site with varying number of ligands, from $Cu(SCH_3)^{0/+}$ to $Cu(SCH_3)(Im)_2(S(CH_3)_2)^{0/+}$, where Im denotes imidazole, are investigated. Following the findings of structural instability in Cu(I) $\times(SCH_3)(Im)_2$ and its stabilization by the addition of the axial methionine (Met) ligand model, the structure and energetics are examined as functions of the $Cu-S_{Met}$ distance in the range of 2.1–3.3 Å. The reorganization energies in both redox states exhibit a minimum at the $Cu-S_{Met}$ distance of ~2.4 Å, whereas the ionization potential increases monotonically. The changes of reorganization energies correlate well with one of the $Cu-N_{His}$ distances rather than the $Cu-S_{Cys}$ distance. The estimated Arrhenius factor for oxidation of plastocyanin by $P700^+$ (in photosystem I) changes by an order of magnitude when the $Cu-S_{Met}$ distance fluctuates between 2.4 and 3.0 Å, whereas the factor for reduction of plastocyanin by cytochrome *f* is nearly constant. Together with the data from our previous classical molecular dynamics simulation of solvated protein, we argue that the electron transfer rate is affected, and thus may be controlled, by the fluctuation of a weakly bound axial Met ligand. We also present the assessment of various exchange-correlation functionals, including those with the long-range correction, against the CCSD(T) reference and on the basis of a perturbative adiabatic connection model. For $Cu(SCH_3)$ and $Cu(SCH_3)(Im)$, simple correlations have been found between the reorganization energies and the amount of Hartree–Fock exchange.
 [doi:10.1063/1.3495983]

I. INTRODUCTION

The redox active site of type 1 blue copper proteins[1–6] contains a copper ion with ligands from a cysteine (Cys) and two histidine (His) residues that form a distorted tetrahedral geometry.[7–10] In many proteins of this type, the fourth ligand is from a methionine (Met) residue ~3 Å away from the copper in the axial direction of the trigonal plane (Fig. 1). The structures observed by x-ray crystallography were very similar between the reduced and the oxidized states,[7–10] in contrast to those in typical inorganic compounds where Cu(I) and Cu(II) tend toward tetrahedral and tetragonal geometries, respectively. The small structural change seemed to imply that the protein environment constrains the active site in ways to reduce the reorganization energy and thereby accelerate the electron transfer.[11–13] This and the related aspects have been also actively examined by synthetic models.[14,15]

These protein regulation hypotheses were, however, challenged by a density functional theory (DFT) calculation.[16] The optimized geometries of the model complex, in which the Cys ligand was replaced by CH_3S^-, His by imidazole, and Met by $(CH_3)_2S$, were close enough to the x-ray structure in both redox states, indicating that the characteristic tetrahedral structure is determined by the local interaction around the copper ion rather than the constraint from the protein environment. This was further supported by combined quantum-mechanics and molecular-mechanics (QM/MM) calculations,[17] which concluded that the blue copper proteins are not more strained than other metalloproteins.

Those results would be simply rationalized in terms of electron delocalization from the Cys thiolate anion that partially reduces the Cu(II) and Cu(I) ions toward both spherical $(3d)^{10}$ and $(3d)^{10}(4s)^1$ configurations that favor isotropic tetrahedral coordination. This picture would thus reduce the relevance of Jahn–Teller distortion. In addition, the nuclear arrangement of the active site only has an approximate symmetry of no higher than C_s.

On the other hand, the roles of the other ligands are less clear. The importance of His ligands was marked in our previous study on ligand-to-metal charge-transfer (LMCT) dynamics in plastocyanin.[18] The major coupling motions to the LMCT excitation were found to include $N_{His}-Cu-N_{His}$ bending and $S_{Cys}-Cu-(N_{His})_2$ wagging motions, whereas the influence of axial Met ligand to the energy spectrum was comparatively minor. Nonetheless, since the redox electron transfer involves smaller energy scale than the LMCT excitation, more detailed analysis would be needed.

The role of axial Met ligand has been studied via mutagenesis, which suggested possibilities of tuning the redox potential and spectroscopic properties and of protecting the metal site from solvent and other external ligands.[3,19] However, there remains an uncertainty about the ligand effect on the reduction potential;[4,20,21] spectroscopic analysis and DFT

a)Electronic mail: ando@kuchem.kyoto-u.ac.jp.

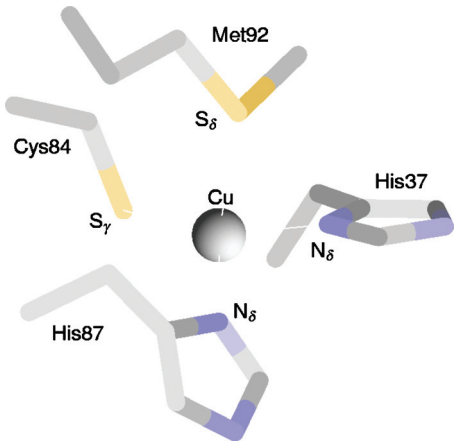

FIG. 1. The active site structure of plastocyanin (from the Protein Data Bank code 1BXU).

X_α calculation first stressed the importance of $Cu-S_{Met}$ distance that modulates the reduction potential by as large as 1 eV,[20] whereas B3LYP DFT calculation predicted an order of magnitude smaller value.[21] More recent spectroscopic analysis with B(38HF)P86 DFT calculation has shown that the reduction potential change should be larger than 200 meV.[22]

With these backgrounds, in this work, we re-examine the role of axial Met ligand. Here, its importance has emerged with the findings of a structural instability in Cu(I)(Cys) $\times(His)_2$ complex and its stabilization by the addition of the axial Met ligand. We shall emphasize the need for investigating both the reduction potential and the reorganization energies. Although there exist many computational works on blue copper proteins, with focus on electronic structure,[16,20,22–27] molecular dynamics,[18,28–30] QM/MM,[17,31–34] electron transfer pathway,[35–38] and docking,[39,40] to our knowledge, none has systematically examined the effect of axial Met ligand on reorganization energies and redox reaction rates.

We also examine various density functionals and the nature of electron correlation in copper complexes. For transition metal complexes, DFT seems promising but yet immature.[41,42] Investigations in this arena are thus important themselves and for advancing QM/MM studies where computational efficiency is the key. Although the popular B3LYP functional[43,44] often yields decent results, its all-round accuracy is not expected as the empirical parameterization excluded transition metal complexes. In such case, a reasonable strategy would be to explore the functionals with smaller number of empirical factors.

Another issue studied here is the long-range correction (LC) in DFT.[45–49] The LC methods are actively developed in the recent years, but their applications to transition metal complexes are yet scarce. The key concept shared between the LC and the hybrid methods is the mixing of Hartree–Fock exchange (HFX) to reduce the self-interaction errors. We analyze this aspect to elucidate the nature of electron correlation in copper complexes. The impact of HFX on geometry optimizations has been examined previously[6] by comparing BP86, B3LYP, and B(38HF)P86 functionals. We systematically extend the analysis with use of the nonempirical Perdew–Burke–Ernzerhof (PBE) functional families and on the ground of a perturbative adiabatic connection model.[50]

Although we are currently working on QM/MM calculations including the protein environment, QM/MM methods intrinsically involve both systematic and statistical errors, as represented by those from the boundary between QM and MM regions. We thus focus in this report on the model complexes, with an aim to establish reference data for comparison with the forthcoming QM/MM results. Under this setting, intriguing pictures have emerged on the potential dynamic role of the weakly bound axial Met ligand.

After summarizing the computational methods in the Sec. II, Sec. III describes the results and discussion. The paper concludes in Sec. IV.

II. COMPUTATIONAL DETAILS

We have selected 17 functionals from 3 criteria. The first is to include those employed in previous related works; the popular B3LYP and the spectroscopically calibrated B(38HF)P86.[51] The second is to include the LC functionals.[46] The third is to employ the functionals with minimal number of empirical parameters; we thus selected PBE (Ref. 52) and RPBE (Ref. 53) for the exchange part and PBE and one-parameter progressive (OP) (Ref. 54) for the correlation part. These are combined to form PBE, RPBE, PBEOP (POP), and RPBEOP (RPOP) functionals. In addition, the hybrids with HFX are examined on the basis of an adiabatic connection model,[50] according to which 50% (1/2) and 25% (1/4) HFX mixtures correspond to the second- and fourth-order perturbation theories (MP2 and MP4), respectively. Hereafter, this model is called "perturbative adiabatic connection model." Following the terminology for PBE0,[55] the other hybrids with 25% HFX will be denoted by RPBE0, POP0, and RPOP0. The hybrids with 50% HFX will be denoted by PBEH, RPBEH, POPH, and RPOPH.

The LANL2DZ(dp) basis set[56,57] was mainly used with effective core potential (ECP) on copper and sulfur. A set of f functions with the exponent 3.525 was added on copper. In some cases, an all-electron basis set was employed for comparison, in which the copper basis set is contracted as (62111111/33111/311) and extended with p, d, and f functions of exponents 0.174, 0.132, and 0.39, and the 6-31G* set is used for the other atoms. This basis set has been used previously[17] and will be denoted as VTZ(Cu)6-31G* hereafter. In all cases, the d and f functions are purified to five and seven functions.

We used the programs GAMESS (Ref. 58) and NWCHEM (Ref. 59) for the electronic structure calculations. The nondefault RPOP functional was implemented with the correlation length parameter $q_{\alpha\beta}$=2.3789, the same value as has been previously determined for the POP functional.[54] The other functionals were also implemented where needed. The two programs have been checked to yield identical results to at least 10^{-4} hartree at given geometries with properly chosen integration grids; the small deviations come from the slight difference in the definition of the grids. The LC-DFT calculations were carried out by GAMESS, and the open-shell

CCSD(T) calculations by NWCHEM.

The parameter μ in the switching function $\mathrm{erf}(\mu r)/r$ of the LC method[46] was taken to be $\mu=0.47$, as has been optimized for ground state properties with the LC-Becke-OP (BOP) functional.[47] The same value was adopted to the LC-POP and LC-RPOP functionals.

The MP2 calculations for the oxidized doublet states were carried out mainly by the Z-averaged (Z-MP2) method[60] from restricted open-shell HF reference. We have also tested the MP2 from unrestricted HF reference (U-MP2) for the smaller two complexes and confirmed that the results are essentially identical for the discussions in this work. We thus employed the less expensive Z-MP2 for the larger complexes. In the MP2 and CCSD(T) calculations, all the orbitals were taken to be active.

The reorganization energies in the reduced and oxidized states, denoted by λ_I and λ_{II}, are calculated from the energy differences at equilibrium geometries; for example, λ_I is defined by the energy cost to deform the system in the reduced state from its optimal geometry to the optimal geometry for the oxidized state.

III. RESULTS AND DISCUSSION

A. Cu(Cys)

We first investigate the minimal complex Cu(Cys), the core part in the active site. Hereafter, the truncated amino acid models, CH_3S^-, $C_3N_2H_4$, and $(CH_3)_2S$, will be denoted by Cys, His, and Met.

The optimized geometrical parameters are listed in Table S1 in the supplementary material (SM).[61] The Cu–S distance is in the range of 214–220 pm in the reduced state and 222–230 pm in the oxidized state. The shorter distance in the reduced state stems from the covalent nature of the Cu(I)–S bond.[20,62] As will be seen in the following sections (Tables S4–S7 in the SM), the difference becomes smaller in the larger complexes with His and Met ligands, and in the Cu(Cys)$(His)_2$(Met) complex the order reverses as observed in the proteins.

The mixing of HFX, e.g., from PBE (0%) to PBE0 (25%) and PBEH (50%), systematically elongates the Cu–S distance and shortens the S–C distance. The same applies to the POP, RPBE, and RPOP families. In comparison, the LC functionals tend to give shorter Cu–S and S–C distances. For the Cu–S–C angle, dispersion among the methods is negligibly small.

The amount of HFX also correlates systematically with the reorganization energies, as plotted in Fig. 2. Data points from B3LYP and B(38HF)P86 are also included and are found to correspond well with the range displayed by the lines from the PBE families. These indicate that the reorganization energies are well characterized by the amount of HFX and are less dependent on the functionals. The horizontal lines were drawn at the values from the LC-BOP functional, to which the results from LC-POP and LC-RPOP were identical within 1 meV. The intersections with the lines from the PBE families indicate that the reorganization energies from the LC functionals correspond to 37%–40% hybrid of HFX. The effect of HFX will be further discussed in Sec. III B.

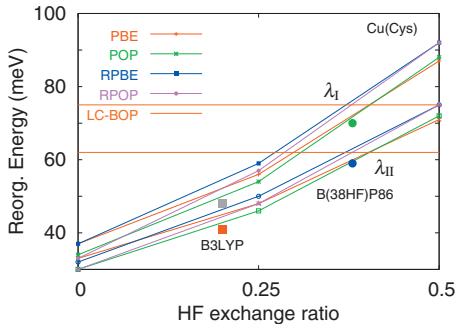

FIG. 2. Reorganization energies vs the amount of Hartree–Fock exchange for Cu(Cys). The lines for λ_I are above those for λ_{II}. The numbers are listed in Table S2 in the Supporting Material (Ref. 61).

The results with different basis sets are summarized in Table S2 in the SM.[61] The replacement of ECP on sulfur by the all-electron DZP basis resulted in negligible changes. On the other hand, the VTZ(Cu)6-31G* basis set tends to give shorter Cu–S distance and smaller reorganization energies. In particular, MP2 with this basis set yielded notably short Cu–S distance of 209 pm in the reduced state. We have checked the calculation by freezing the lowest 15 (chemical core) orbitals and found no significant change. In the following, we mainly employ the LANL2DZ(dp) set with ECPs on copper and sulfur, as it appears qualitatively sufficient and well-balanced. We will revisit the VTZ(Cu)6-31G* set in Sec. III D.

B. Perturbative adiabatic connection model

Here, we describe an analysis based on the perturbative adiabatic connection model. According to this model, the 50% hybrids (PBEH, POPH, RPBEH, and RPOPH) correspond to MP2. The Z-MP2 calculations yielded the reorganization energies $\lambda_I=99$ meV and $\lambda_{II}=82$ meV. Comparison of these with Fig. 2 confirms that the 50% hybrids certainly give the reorganization energies closest to the MP2 values.

If we therefore trust this model, the 25% hybrids should correspond to MP4. Generally, the MP4 calculations are more expensive than the coupled-cluster methods, while the accuracy is in the order of CCSD < MP4 < CCSD(T). We thus computed CCSD(T) energies at the geometries optimized by the DFT methods. The results are listed in Table S3 in the SM.[61] With one exception (PBE0 and PBEH in oxidized state), the geometries from the 25% hybrid functionals yielded lower CCSD(T) energies than those from the 50% hybrids, indicating that the former is more reliable for structural calculations. The lowest CCSD(T) energy is found at the RPOP0 geometries for both redox states. The CCSD(T) reorganization energies from the RPOP0 geometries are 62 meV in both states.

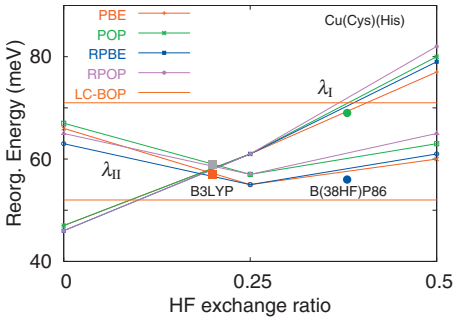

FIG. 3. The same as in Fig. 2 but for Cu(Cys)(His). The nearly straight lines are for λ_I whereas the V-shaped ones are for λ_{II}. The numbers are listing in Table S4 in the Supporting Material (Ref. 61).

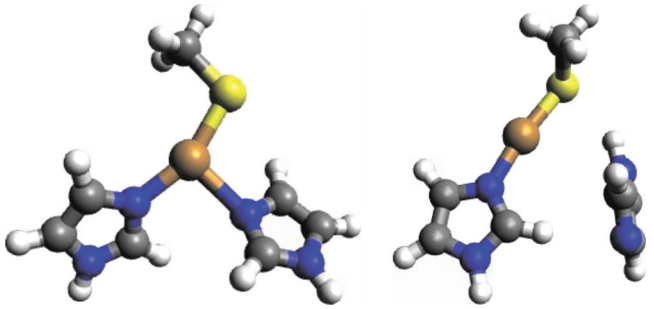

FIG. 4. Optimized structure of Cu(I)(Cys)$(His)_2$ by PBE0 (left, trigonal) and B3LYP (right, T-shape) functionals.

C. Cu(Cys)(His)

We now add a His model to the minimal complex. The optimized geometries show linear arrangement of the S–Cu–N atoms in both reduced and oxidized states. The plane formed by the $Cu-S-C_{Cys}$ atoms and the molecular plane of His are perpendicular to each other in the reduced state, whereas they are parallel to each other in the oxidized state [Fig. S1 in the SM (Ref. 61)]. These structures can be interpreted in terms of balance between electrostatic repulsion and conjugation between the lone pair orbital on sulfur and the π orbitals of His; by removing an electron from the highest occupied molecular orbital (HOMO), which mainly consists of the sulfur lone pair orbital, the electrostatic repulsion is reduced and the conjugation is enhanced.

The linear structures of Cu(Cys)(His) contrast with the trigonal structures in the larger complexes with two His ligands that are seen in the protein active site and in the next sections. This implies absence of strong directionality in the $Cu-N_{His}$ ligand bonds, in accord with the picture of nearly spherical electronic configurations on Cu, as mentioned in Sec. I. Indeed, from the natural population analysis (NPA) (Ref. 63) the effective charge on Cu site was typically 0.5–0.7 in the reduced state and 0.7–0.9 in the oxidized state.

The reorganization energies λ_I and λ_{II} along the amount of HFX are plotted in Fig. 3. λ_I increases almost linearly, similar to the case of Cu(Cys) in Fig. 2, but the slope is smaller. The His ligand thus moderates the effect of HFX. On the other hand, the behavior of λ_{II} is qualitatively different; all the lines are V-shaped and the overall change along the HFX is smaller. These behaviors of λ_I and λ_{II} appear to correlate with the change of Cu–S distance. That is, $\lambda_I(\lambda_{II})$ depends mostly on the structures in the oxidized (reduced) state, and as listed in Table S4 in the SM,[61] the Cu–S distance increases systematically along the HFX in the oxidized state, but not in the reduced state.

D. Cu(Cys)$(His)_2$

The addition of the second His ligand induces notable changes. Hereafter, the nitrogen atoms corresponding to the N_δ in His37 and His87 in Fig. 1 are denoted by N_a and N_b.

The optimized structural parameters and the reorganization energies are listed in Table S5 in the SM.[61] Noted, in particular, is the dispersion among different functionals of the $Cu-N_b$ distance in the reduced state. The structures are grouped into two types: trigonal (Fig. 4) and T-shape (Fig. 4). The latter contains a Cu(Cys)(His) part in a linear structure, similar to that found in Sec. III C, and the other His located with large (>4 Å) $Cu-N_b$ distance. The trigonal structure was found by MP2, B(38HF)P86, PBE0, PBEH, POPH, RPBEH, and all the LC functionals, whereas the T-shape structure was obtained by the remaining functionals, B3LYP, PBE, POP, POP0, RPBE, RPBE0, RPOP, RPOP0, and RPOPH. Comparison in the PBE families indicates that the larger amount of HFX tends to stabilize the trigonal structure. This is also seen in the results from the three LC functionals that commonly yielded the trigonal structure.

The corresponding results from the VTZ(Cu)6-31G* basis set are listed in Table S6 in the SM.[61] They show similar tendency to the LANL2DZ(dp) set, but with a few more cases giving the T-shape structure in the PBE families. For both basis sets, B3LYP gives the T-shape structure whereas B(38HF)B86 gives the trigonal structure. This again appears to correlate with the amount of HFX.

Further analysis has revealed that the T-shape structure is generally more stable and, in some cases, the trigonal structure corresponds to a metastable local minimum. This is shown in Fig. 5, which plots the minimum energy profiles along the $Cu-N_b$ distance. Again, the amount of HFX appears to correlate with the energy profiles in the short $Cu-N_b$ distance (<2.4 Å); the energy is uphill for B(38HF)P86 and the LC functionals, whereas it is downhill for B3LYP, POP0, RPBE0, and RPOP0. The behavior in this region is closely related to the ligand reorganization. Comparison with the CCSD(T) results[64] in Fig. 5 shows that the former group tends to overestimate the Cu-His binding, whereas the latter group underestimates. Figure 5 also shows that the best agreement with the CCSD(T) reference in the short distance region is obtained by PBE0, and the second best is by B3LYP.

These results are suggestive of the nature of electron correlation in copper complex. In general, major errors in DFT come from poor cancellation of the self-interaction in the Coulomb and exchange energy terms, which is improved by the introduction of HFX that partially removes the self-exchange. The results in Fig. 5 implies that the uniform introduction of 25% HFX undercounts the self-interaction correction to POP, RPBE, and RPOP functionals, whereas the LC with μ=0.47 overcounts. The LC functionals may be calibrated by adjusting the switching parameter μ since the smaller μ reduces the amount of HFX in the short-range

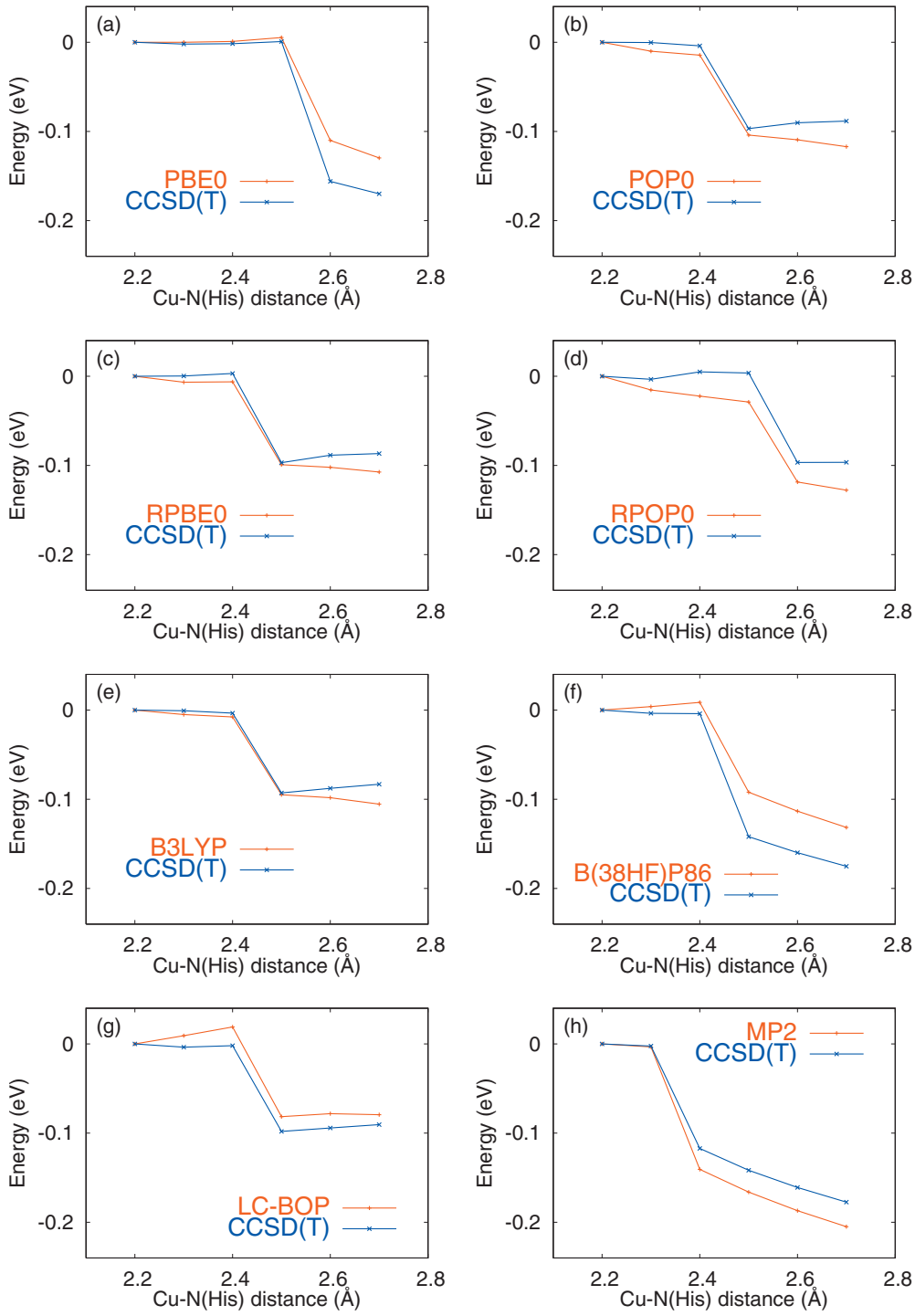

FIG. 5. Energy of $Cu(Cys)(His)_2$ along the $Cu-N_b$ distance. The coordinates other than the $Cu-N_b$ distance were relaxed by the DFT methods. Superimposed in each figure are the CCSD(T) energies calculated at the corresponding DFT geometries.

region. (Note that the original optimization to μ=0.47 excluded transition metal complexes.[47]) However, we shall not pursue this calibration in the present work.

The qualitative observations here may be related to the "hard-soft" concept of the metal-ligand interaction; the soft Cu(I) ion does not fit well with the moderately hard ligands such as His nitrogen and thus tend to repel one of the His ligands. In the oxidized state, on the other hand, the trigonal structure was obtained by all the functionals and MP2, which seems in accord with the hardness of the Cu(II) ion as well as with the stronger electrostatic interaction.

Because of the structural irregularity observed in the reduced state, the reorganization energies and the amount of HFX no longer show systematic correlation. Nonetheless, the moderation due to the His ligand, as discussed in Sec. III C for Cu(Cys)(His), seems to carry over.

E. $Cu(Cys)(His)_2(Met)$

It was found that the structural instability of $Cu(I)(Cys)(His)_2$ is quenched by the addition of a Met ligand in the axial position. The optimized structural parameters are

listed in Table S7 in the SM.[61] Starting from the x-ray structure, all but one (RPOP) functionals yielded trigonal geometry of the Cu(I)(Cys)$(His)_2$ part. Comparison with the results in Sec. III D thus indicates that the axial Met ligand stabilizes the trigonal structure.

There exists, however, dispersion of the optimized $Cu-S_{Met}$ distance. It is less than 3 Å for MP2, B(38HF)P86, PBE, PBE0, PBEH, RPBE0, RPBEH, and the LC functionals, whereas it is longer than 4.5 Å for the remaining functionals including B3LYP, POP, POP0, POPH, RPBE, RPOP, RPOP0, and RPOPH. This grouping roughly corresponds to that into the trigonal and T-shape structures for the Cu(I) $\times$(Cys)$(His)_2$ complex in Sec. III D.

Interestingly, the best two functionals discussed in Sec. III D from the results in Fig. 5, PBE0 and B3LYP, belong to the different groups. We thus compared the CCSD(T) energies at their optimized geometries and found that the PBE0 geometry is more stable by 109 meV than the B3LYP geometry; this indicates that the former functional yields more reliable interactions and structures. We will thus use the PBE0 functional for the extensive calculations in the next section.

The stabilization of the trigonal structure induced by Met ligand may be again interpreted in terms of the hard-soft concept. The soft thioether group of Met interacts well with the soft Cu(I) ion. Then, the induced electronic polarization "hardens" the Cu(I) ion and stabilizes the two His ligands. This picture is supported by the NPA on the Cu(I) site, which was found more positive in Cu(I)(Cys)$(His)_2$(Met) than in Cu(I)(Cys)$(His)_2$. Indeed, the effective charge on the Cu site increases monotonically with increasing the number of ligands from Cu(Cys) to Cu(Cys)$(His)_2$(Met) in the reduced state: 0.541, 0.562, 0.653, and 0.696. The corresponding change in the oxidized state was not monotonic: 0.796, 0.703, 0.913, and 0.892. The structure in the oxidized state is robust; it is tetrahedral by all the functionals and MP2, and the $Cu-S_{Met}$ distance was in the range of 2.4–2.6 Å.

F. Reorganization control by Met

The results in the previous sections illuminate the importance of axial Met ligand in determining the active site structure. This further suggests that the Met ligand may control the structural reorganization in the redox reaction. We thus examine the structure and energy as functions of the $Cu-S_{Met}$ distance. The calculations were repeated by constraining the $Cu-S_{Met}$ distance at values between 2.1 and 3.3 Å but the other coordinates relaxed. As decided in Secs. III D and III E with reference to the CCSD(T) calculations, the PBE0 functional is employed in this section.

Figure 6(a) plots the reorganization energies along the $Cu-S_{Met}$ distance. The average $\lambda_{av}=(\lambda_I+\lambda_{II})/2$ is also included. All of them show a minimum $\lambda \simeq 0.22$ eV at 2.4 Å and increases up to 0.45 eV at 3.3 Å. The range of $Cu-S_{Met}$ distance observed by x-ray crystallography for various blue copper proteins is 2.5–3.3 Å. In this regard, the proteins do not necessarily constrain the $Cu-S_{Met}$ distance simply to *minimize* the reorganization energy. Instead, the constraint may *control* the reorganization energy and thus the electron transfer rate; this will be discussed further below.

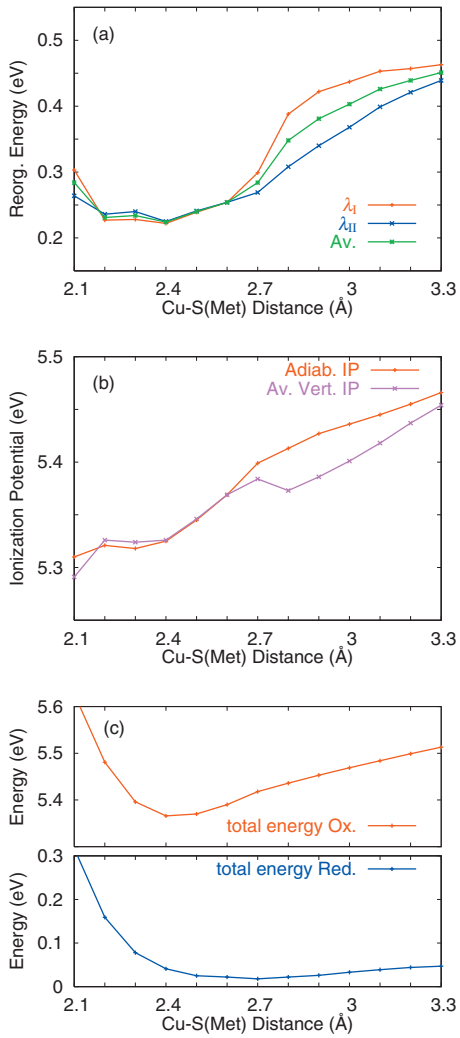

FIG. 6. Reorganization energies, ionization potentials, and total energies of Cu(Cys)$(His)_2$(Met) along the $Cu-S_{Met}$ distance.

The computed ionization potentials (IPs) are plotted in Fig. 6(b). The adiabatic IP and the average of two vertical IPs are included. They increase monotonically along the $Cu-S_{Met}$ distance, from ~5.31 eV at 2.1 Å to 5.47 eV at 3.3 Å for the adiabatic IP. This increase of 160 meV is closer to the recent estimate of 200 meV (Ref. 22) than to the previous prediction of 70 meV by B3LYP.[21]

The changes of the reorganization energy, 230 meV, and of the IP, 160 meV, are in comparable magnitude. These are non-negligible for the inner-sphere reorganization energy in electron transfer reactions. Moreover, it is these comparable energies that bring about the qualitatively notable difference between the oxidation and reduction processes, as will be discussed in the next section. Although the influence of the protein environment should be examined with care, it seems generally unlikely for the inner-sphere metal-ligand energies as large as 200 meV to be masked or smeared out.[65]

The total energies along the $Cu-S_{Met}$ distance are plotted in Fig. 6(c). The curve in the reduced state shows a minimum at $Cu(I)-S_{Met}$ distance 2.7 Å and is very flat, within 300 $K \simeq 26$ meV in the range of 2.4–3.1 Å. On the other hand, the potential in the oxidized state exhibits a

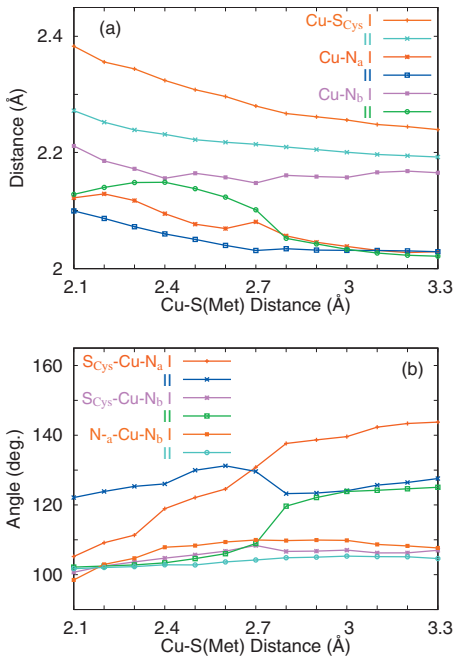

FIG. 7. Changes of the structural parameters in $Cu(Cys)(His)_2(Met)$ along the $Cu-S_{Met}$ distance.

deeper well with the minimum at $Cu(II)-S_{Met}$ distance of ~2.4 Å, in agreement with previous works.[16,22,62]

The changes of $Cu-S_{Cys}$ and two $Cu-N_{His}$ distances are plotted in Fig. 7(a). In both redox states, the $Cu-S_{Cys}$ shortens as the $Cu-S_{Met}$ elongates. However, the difference between the redox states becomes smaller along $Cu-S_{Met}$, indicating that the change of $Cu-S_{Cys}$ is not the origin of the increase of the reorganization energy.

It was previously argued that the decrease of $Cu-S_{Cys}$ is the origin of the increase of reduction potential along $Cu-S_{Met}$.[19,20,22] This does not conflict with the present results but implies that the origins of the changes of reduction potential and of reorganization energy are different. The reduction potential depends mostly on the $Cu-S_{Cys}$ distance as the HOMO mainly consists of the lone pair orbital of S_{Cys}. In contrast, Fig. 7(a) shows that the reorganization of $Cu-N_b$ distance is most likely the origin of the increase of reorganization energy, as its difference between the redox states increases along $Cu-S_{Met}$ beyond 2.4 Å. On the other hand, the difference of $Cu-N_a$ between the redox states decreases along $Cu-S_{Met}$.

The most visible structural change along $Cu-S_{Met}$ is the flattening of the $Cu(Cys)(His)_2$ part. This is seen in Fig. 7(b), where the sum of $N_{His}-Cu-N_{His}$ and two $S_{Cys}-Cu-N_{His}$ angles approaches to 360° in both redox states. The two $S_{Cys}-Cu-N_{His}$ angles do not correlate well with the reorganization energies in Fig. 7(a), and the $N_{His}-Cu-N_{His}$ angle does not change much along $Cu-S_{Met}$. These imply that these angles do not contribute much to the reorganization energy. This last conclusion is qualitatively consistent with the normal mode analysis[20] and with the picture of nearly spherical electronic configuration on Cu as mentioned in Sec. I.

G. Estimating the Arrhenius factor

According to the linear response model, the activation free energy of redox electron transfer is given by[66,67]

$$\Delta G^{\ddagger} = \frac{(\Delta G^0 + \lambda)^2}{4\lambda}, \tag{1}$$

where ΔG^0 is the reaction free energy. ΔG^0 is evaluated from the difference of the reduction potentials of the donor and the acceptor. For example, the reduction potentials versus the standard normal hydrogen electrode (NHE) of *P. nigra* plastocyanin (Pc), cytochrome *f* (cyt*f*), and the $P700^+$ (in photosystem I) are experimentally determined as $E^0(Pc) = 370$ mV, $E^0(cytf) = 340$ mV, and $E^0(P700^+) = 490$ mV,[5] respectively. Thus, the reaction free energy for the reduction of Pc by cyt*f* is $\Delta G^0_{red}/e = E^0(cytf) - E^0(Pc) = -30$ mV, and that for the oxidation of Pc by $P700^+$ is $\Delta G^0_{ox}/e = E^0(Pc) - E^0(P700^+) = -120$ mV. Note that $E^0(Pc)$ enters in ΔG^0_{Red} and ΔG^0_{Ox} in different signs.

The reduction potential of Pc is related to its IP via

$$E^0(Pc) = IP/e - E_{NHE} + E_c, \tag{2}$$

in which E_{NHE} is a conversion constant to the NHE scale and E_c contains the other factors, such as solvation contribution. Here, we set $E_{NHE} = 4.5$ V and calibrate E_c from the computed IP and the experimental $E^0(Pc)$. From Fig. 6(b), we find IP=5.42 eV at $Cu-S_{Met}$ distance of 2.87 Å, the observed distance from x-ray crystallography of *P. nigra* Pc.[9] Using this IP, we obtain $E_c = -0.55$ V. Using Eq. (2) and Fig. 6(b), ΔG^0_{Red} and ΔG^0_{Ox} are evaluated as functions of the $Cu-S_{Met}$ distance.

For the reorganization energy λ, we use the results in Fig. 6(a). Since the reorganization energies in Fig. 6(a) represent only the inner-sphere part of Pc, we need to estimate contributions from the protein environment, the donor cyt*f*, and the acceptor $P700^+$. The previous QM/MM study[17] showed that the protein environment reduces the inner-sphere reorganization energy by reducing the change of metal-ligand bonds. The Car–Parrinello QM/MM molecular dynamics calculation[32] evaluated the inner-sphere reorganization energy as small as 0.1 eV, and the outer-sphere reorganization energy of 0.6 eV. This latter value mainly comes from the solvent water, and the protein reorganization was reported to be negligible. However, the solvent reorganization energy may be mostly excluded at the docking conformation of the redox proteins. Considering these, we assume that the electrostatic effect from the protein environment shift the curve in Fig. 6(a) downward by 0.2 eV. We also assume that the reorganization energies in cyt*f* and P700 are about 0.2 eV. The uncertainty in these estimates will be taken into account in the calculations below.

The calculated Arrhenius factors, $\exp(-\Delta G^{\ddagger}/k_B T)$, at the room temperature are plotted in Fig. 8. To take account of the uncertainty in the evaluation of reorganization energy and to check the robustness of the conclusion, calculations with the λ_{av} shifted by +0.1 eV are also included. Particularly noted is the large dependence on the $Cu-S_{Met}$ distance for the oxidation of Pc by $P700^+$. For example, the factor at 2.4 Å $Cu-S_{Met}$ is 8.6 times larger than that at 3.0 Å. This ratio is

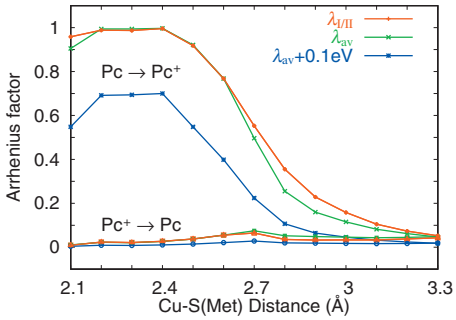

FIG. 8. The Arrhenius factors for oxidation and reduction of plastocyanin by $P700^+$ and cytochrome *f* as functions of the $Cu-S_{Met}$ distance.

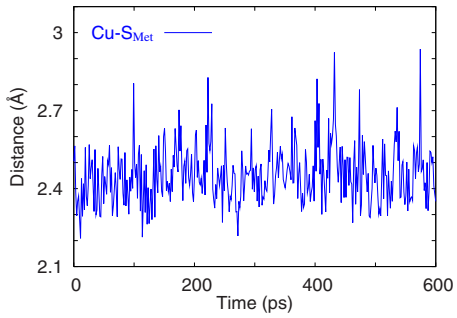

FIG. 9. A molecular dynamics trajectory of Cu(II)-S_{Met} distance in a solvated plastocyanin.

even greater, 15.2, with the use of $\lambda_{av}+0.1$ eV. Moreover, it is this process in which the potential along $Cu-S_{Met}$ is flatter [Fig. 6(c)], and thus the larger fluctuation of $Cu-S_{Met}$ is expected. For the reduction of Pc^+ by cyt*f*, on the other hand, the Arrhenius factor does not change much along $Cu-S_{Met}$.

The large difference between the reduction and oxidation processes can be understood simply via linear approximation, $\lambda(R) \simeq \lambda(R_0)+a(R-R_0)$ and $IP(R) \simeq IP(R_0)+b(R-R_0)$, where R and R_0 denote the $Cu-S_{Met}$ distance and its representative value, e.g., $R_0=2.9$ Å. As seen in Figs. 6(a) and 6(b), both a and b are positive around $R_0=2.9$ Å. The point here is that the IP(Pc) enters in ΔG^0_{red} and ΔG^0_{ox} in different sign, and thus the numerator in Eq. (1) has a different dependence on R with the slope $(a-b)$ for the reduction of Pc^+ and $(a+b)$ for the oxidation of Pc.

IV. CONCLUDING REMARKS

The pictures emerging from the last two sections are summarized as follows. (1) The reduction potential is chiefly determined by the Cu(Cys) part (as the major component of HOMO is the sulfur lone pair), whereas the local (ligand) reorganization energy is mainly controlled by the Cu-His interaction. In these regards, therefore, the Cys and His ligands have different roles in the redox electron transfers. Moreover, these may be controlled by the Met ligand, as will be described next. (2) In the oxidation of Pc by $P700^+$, not only the $Cu-S_{Met}$ distance is flexible, but also the electron transfer rate is sensitive to it; the Arrhenius factor can change by an order of magnitude when the $Cu-S_{Met}$ distance fluctuates in the thermally accessible range. On the other hand, in the reduction of Pc^+ by cyt*f*, not only the $Cu-S_{Met}$ distance is more constrained, but also its influence on the Arrhenius factor is much smaller.

To elucidate the dynamical fluctuation of the methionine ligand, the effects of the protein environment should be important. This aspect is currently under study by the QM/MM method. Nonetheless, in order to sketch the idea, we display in Fig. 9 a trajectory of the $Cu(II)-S_{Met}$ distance from our previous classical molecular dynamics simulation of solvated plastocyanin.[18] As seen, it exhibits a diffusive and large amplitude fluctuation in the range corresponding to Figs. 6–8. The diffusive behavior is also observed in the sharp decay of its time-correlation function and its broad spectrum, the characteristics of white noise, as has been presented in Figs. 4b and 5a of Ref. 18. The $Cu(I)-S_{Met}$ distance will also behave a diffusive fluctuation on an even flatter potential surface [Fig. 7(c)]. In such case, the diffusion-reaction model such as the Sumi–Marcus model[68–70] would be applicable. As demonstrated by the Sumi–Marcus theory, the diffusion-controlled electron transfer may exhibit multiple time-scale kinetics. Its relevance to the physiological electron transfer by blue copper proteins would be an intriguing issue to explore. Works along this line will be reported in the future.

ACKNOWLEDGMENTS

This work was supported by KAKENHI in Innovative Areas (Grant No. 20108017, "π-space").

[1] H. B. Gray and E. I. Solomon, *Copper Proteins* (Wiley, New York, 1981).
[2] A. G. Sykes, Adv. Inorg. Chem. **36**, 377 (1991).
[3] D. S. Wuttke and H. B. Gray, Curr. Opin. Struct. Biol. **3**, 555 (1993).
[4] B. G. Malmström and J. Leckner, Curr. Opin. Chem. Biol. **2**, 286 (1998).
[5] H. B. Gray, B. G. Malmström, and R. J. P. Williams, JBIC, J. Biol. Inorg. Chem. **5**, 551 (2000).
[6] E. I. Solomon, R. K. Szilagyi, S. D. George, and L. Basumallik, Chem. Rev. (Washington, D.C.) **104**, 419 (2004).
[7] P. M. Colman, H. C. Freeman, J. M. Guss, M. Murata, V. A. Norris, J. A. M. Ramshaw, and M. P. Venkatappa, Nature (London) **272**, 319 (1978).
[8] J. M. Guss, P. R. Harrowell, M. Murata, V. A. Norris, and H. C. Freeman, J. Mol. Biol. **192**, 361 (1986).
[9] J. M. Guss, H. D. Bartunik, and H. C. Freeman, Acta Crystallogr., Sect. B: Struct. Sci. **48**, 790 (1992).
[10] T. Inoue, H. Sugawara, S. Hamanaka, H. Tsukui, E. Suzuki, T. Kohzuma, and Y. Kai, Biochemistry **38**, 6063 (1999).
[11] B. G. Malmström, Eur. J. Biochem. **223**, 711 (1994).
[12] R. J. P. Williams, Eur. J. Biochem. **234**, 363 (1995).
[13] P. Wittung-Stafshede, M. G. Hill, E. Gomez, A. J. D. Bilio, B. G. Karlsson, J. Leckner, J. R. Winkler, H. B. Gray, and B. G. Malmström, JBIC, J. Biol. Inorg. Chem. **3**, 367 (1998).
[14] K. Fujisawa, K. Fujita, T. Takahashi, N. Kitajima, Y. Moro-oka, Y. Matsunaga, Y. Miyashita, and K. Okamoto, Inorg. Chem. Commun. **7**, 1188 (2004).
[15] S. I. Gorelsky, L. Basumallick, J. Vura-Weis, R. Sarangi, K. O. Hodgson, B. Hedman, K. Fujisawa, and E. I. Solomon, Inorg. Chem. **44**, 4947 (2005).
[16] U. Ryde, M. H. M. Olsson, K. Pierloot, and B. O. Roos, J. Mol. Biol. **261**, 586 (1996).
[17] U. Ryde and M. H. M. Olsson, Int. J. Quantum Chem. **81**, 335 (2001).
[18] K. Ando, J. Phys. Chem. B **112**, 250 (2008).
[19] D. W. Randall, D. R. Gamelin, L. B. LaCroix, and E. I. Solomon, JBIC, J. Biol. Inorg. Chem. **5**, 16 (2000).
[20] J. A. Guckert, M. D. Lowery, and E. I. Solomon, J. Am. Chem. Soc. **117**, 2817 (1995).
[21] M. H. M. Olsson and U. Ryde, JBIC, J. Biol. Inorg. Chem. **4**, 654 (1999).
[22] S. Ghosh, X. Xie, A. Dey, Y. Sun, C. P. Scholes, and E. I. Solomon, Proc. Natl. Acad. Sci. U.S.A. **106**, 4969 (2009).
[23] S. Larsson, A. Broo, and L. Sjölin, J. Phys. Chem. **99**, 4860 (1995).
[24] K. Pierloot, J. O. A. D. Kerpel, U. Ryde, M. H. M. Olsson, and B. O. Roos, J. Am. Chem. Soc. **120**, 13156 (1998).

[25] S. Corni, F. D. Rienzo, R. D. Felice, and E. Molinari, Int. J. Quantum Chem. **102**, 328 (2005).
[26] M. Cascella, M. A. Cuendet, I. Tavernelli, and U. Rothlisberger, J. Phys. Chem. B **111**, 10248 (2007).
[27] M. Pavelka and J. V. Burda, Mol. Phys. **106**, 2733 (2008).
[28] L. W. Ungar, N. F. Scherer, and G. A. Voth, Biophys. J. **72**, 5 (1997).
[29] D. M. Lockwood, Y. K. Cheng, and P. J. Rossky, Chem. Phys. Lett. **345**, 159 (2001).
[30] D. N. LeBard and D. V. Matyushov, J. Phys. Chem. B **112**, 5218 (2008).
[31] M. H. M. Olsson, G. Hong, and A. Warshel, J. Am. Chem. Soc. **125**, 5025 (2003).
[32] M. Cascella, A. Magistrato, I. Tavernelli, P. Carloni, and U. Rothlisberger, Proc. Natl. Acad. Sci. U.S.A. **103**, 19641 (2006).
[33] K. Paraskevopoulos, M. Sundararajan, R. Surendran, M. A. Hough, R. R. Eady, I. H. Hillier, and S. S. Hasnain, Dalton Trans. **2006**, 3067.
[34] J. Kang, T. Ohta, Y. Hagiwara, K. Nishikawa, T. Yamamoto, H. Nagao, and M. Tateno, J. Phys.: Condens. Matter **21**, 064235 (2009).
[35] H. E. M. Christensen, L. S. Conrad, K. V. Mikkelsen, M. K. Nielsen, and J. Ulstrup, Inorg. Chem. **29**, 2808 (1990).
[36] T. Kawatsu, T. Kakitani, and T. Yamato, J. Phys. Chem. B **106**, 11356 (2002).
[37] C. Kobayashi, K. Baldridge, and J. N. Onuchic, J. Chem. Phys. **119**, 3550 (2003).
[38] S. S. Skourtis, I. A. Balabin, T. Kawatsu, and D. N. Beratan, Proc. Natl. Acad. Sci. U.S.A. **102**, 3552 (2005).
[39] G. M. Ullmann, E. W. Knapp, and N. M. Kostić, *Charge Transfer Processes in Condensed Media* (Springer, Berlin, 1979).
[40] A. R. Bizzarri, E. Brunori, B. Bonanni, and S. Cannistraro, Physica A **267**, 257 (1999).
[41] J. N. Harvey, Annu. Rep. Prog. Chem., Sect. C: Phys. Chem. **102**, 203 (2006).
[42] C. J. Cramer and D. G. Truhlar, Phys. Chem. Chem. Phys. **11**, 10757 (2009).
[43] A. D. Becke, J. Chem. Phys. **98**, 5648 (1993).
[44] P. J. Stephens, F. J. Devlin, C. F. Chablowski, and M. J. Frisch, J. Phys. Chem. **98**, 11623 (1994).
[45] T. Leininger, H. Stoll, H. J. Werner, and A. Savin, Chem. Phys. Lett. **275**, 151 (1997).
[46] H. Iikura, T. Tsuneda, T. Yanai, and K. Hirao, J. Chem. Phys. **115**, 3540 (2001).
[47] J. W. Song, T. Hirosawa, T. Tsuneda, and K. Hirao, J. Chem. Phys. **126**, 154105 (2007).
[48] A. V. Krukau, G. E. Scuseria, J. P. Perdew, and A. Savin, J. Chem. Phys. **129**, 124103 (2008).
[49] J. W. Song, M. A. Watson, and K. Hirao, J. Chem. Phys. **131**, 144108 (2009).
[50] J. P. Perdew, M. Ernzerhof, and K. Burke, J. Chem. Phys. **105**, 9982 (1996).
[51] R. K. Szilagyi, M. Metz, and E. I. Solomon, J. Am. Chem. Soc. **106**, 2994 (2002).
[52] J. P. Perdew, K. Burke, and M. Ernzerhof, Phys. Rev. Lett. **77**, 3865 (1996).
[53] B. Hammer, L. B. Hansen, and J. K. Nørskov, Phys. Rev. B **59**, 7413 (1999).
[54] T. Tsuneda, T. Suzumura, and K. Hirao, J. Chem. Phys. **110**, 10664 (1999).
[55] C. Adamo and V. Barone, J. Chem. Phys. **110**, 6158 (1999).
[56] C. E. Check, T. O. Faust, J. M. Bailey, B. J. Wright, T. M. Gilbert, and L. S. Sunderlin, J. Phys. Chem. A **105**, 8111 (2001).
[57] We adjusted the GAMESS input to the LANL2DZdp basis set in the NWCHEM library. Care has been taken for the hydrogen DZV basis in GAMESS, which is different from the LANL2DZ basis in the NWCHEM library.
[58] M. W. Schmidt, K. K. Baldridge, J. A. Boatz, S. T. Elbert, M. S. Gordon, J. H. Jensen, S. Koseki, N. Matsunaga, K. A. Nguyen, S. J. Su, T. L. Windus, M. Dupuis, and J. A. Montgomery, J. Comput. Chem. **14**, 1347 (1993).
[59] E. J. Bylaska, W. A. de Jong, N. Govind, K. Kowalski, T. P. Straatsma, M. Valiev, D. Wang, E. Aprà, T. L. Windus, J. Hammond *et al.*, NWCHEM, a computational chemistry package for parallel computers, version 5.1.1, Pacific Northwest National Laboratory, Richland, Washington 99352-0999, 2009.
[60] T. J. Lee, A. P. Rendell, K. G. Dyall, and D. Jayatilaka, J. Chem. Phys. **100**, 7400 (1994).
[61] See supplementary material at http://dx.doi.org/10.1063/1.3495983 for the tables of the optimized structural parameters and reorganization energies for the Cu(Cys) to Cu(Cys)$(His)_2$(Met) complexes, the table of CCSD(T) energies of Cu(Cys) at the geometries optimized by DFT, and the figures of the optimized structures of Cu(Cys)(His).
[62] K. Ando, J. Phys. Chem. B **108**, 3940 (2004).
[63] A. E. Reed, L. A. Curtis, and F. Weinhold, Chem. Rev. (Washington, D.C.) **88**, 899 (1988).
[64] The T_1 diagnostic of the CCSD(T) calculation was in the range of 0.191–0.196 and did not change much along the Cu–N_b distance. The moderately high values are likely due to the orbital relaxation coming from the so-called "double-shell" effect, which is not expected to affect much the energy profiles in the plots.
[65] In order to resolve this issue, we anticipate that substantially improved QM(DFT)/MM methodologies would be needed, on which we are currently elaborating.
[66] R. A. Marcus, J. Chem. Phys. **24**, 979 (1956).
[67] R. Kubo and Y. Toyozawa, Prog. Theor. Phys. **13**, 160 (1955).
[68] H. Sumi and R. A. Marcus, J. Chem. Phys. **84**, 4894 (1986).
[69] H. Sumi, Adv. Chem. Phys. **107**, 601 (1999).
[70] K. Ando and H. Sumi, J. Chem. Phys. **118**, 8315 (2003).